

Contents lists available at ScienceDirect

Chemical Engineering Research and Design



journal homepage: www.elsevier.com/locate/cherd



Mass transfer phenomena of partially miscible liquids under liquid-liquid slug flow in a circular microchannel

Aloisiyus Yuli Widianto^{*}, Virginia Lorenza, Cindy Clarisa, Reynaldo Valentino, Caroline Elfa, Lanny Sapei

Chemical Engineering-University of Surabaya, Jl. Raya Kalirungkut, Surabaya 60293, Indonesia

ARTICLE INFO

Keywords:
Microreactor
Mass transfer
Slug flow
Two-phase flow
Specific surface area

ABSTRACT

Microreactors have been demonstrated to become an effective tool for increasing mass and heat transfer in heterogeneous chemical processes that are unachievable in batch or continuous stirred tank reactors. The key to superior performance is the availability of a large specific surface area (A/V) in the microsystem for mass and heat transfer between phases. Among the flow patterns generated in the two-phase liquid-liquid flow, slug is an ideal flow with a high stability characteristic, regular velocity, and uniform dimension throughout a micro-channel system. The flow behavior gives slugs great potential to increase mass and heat transfer between phases, so optimizing the utilization of microreactors in many chemical process applications needs an in-depth understanding of the liquid-liquid hydrodynamic. Therefore, the current work aims to determine the mass transfer coefficient under liquid-liquid slug flow and the influence of slug dimensions, channel material, volumetric flow rate, and the flow rate ratio of the organic-aqueous phase on the mass transfer coefficient. The experiments were performed in 1 mm (ID) circular PTFE and silicone tubes, with a 30–40 ml/hour flow rate, and sodium hydroxide concentrations of 0.1, 0.13, and 0.15 M were used. The results exhibit that the most prominent overall mass transfer coefficient was 0.121/s, attained at 0.15 M sodium hydroxide concentration, with 40 ml/hour total discharge within the silicone channel. Microchannels generated smaller slug sizes at a higher aqueous phase flow rate than the organic phase. The smaller size provided a large specific surface area (A/V) for enhancing the mass transfer coefficient.

1. Introduction

Microdevice technology plays an increasingly important role nowadays and has many positive impacts on the development of science and industrial applications. One of the rapidly developing fields in microtechnology is microstructure reactors (microreactors). Microreactors consist of several channels with an inner diameter of less than 1 mm (Prakash and Ghosh, 2021; Zhang et al., 2019). Because of the small dimension, the surface area (A) to volume (V) ratio that can be provided on a micro-scale under a hydraulic diameter range of ten to hundreds of micrometers is very high, attaining $10,000-50,000~\text{m}^2/\text{m}^3$ (Dessimoz et al., 2008), a much greater value than conventional reactors which are only able to provide $100-400~\text{m}^2/\text{m}^3$ (Jähnisch et al., 2004). The high surface area to volume ratio is a crucial aspect required for enhancing mass and heat transfer performance between phases in a unit process. The huge specific surface found in a microfluidic system is able to encourage the provision of a high mass and heat transfer coefficients up

to 1.1/s (Ratchananusorn et al., 2011) and 25,000 W/m².K, respectively, which allows intensification of highly exothermic and or endothermic takes place effectively (Dessimoz et al., 2008; Wang et al., 2020; Ghaini et al., 2010).

The hydrodynamic of two-phase microfluidic systems has three different aspects to be considered: the first, the surface area to volume ratio; the second, the flow is characterized by a small Capillary number (C_a) , which expresses that the influence of surface tension force is more predominant than viscous force in the system; and the third, microroughness and wettability channel wall exert significant influence to the formation of flow pattern. In a laminar multiphase flow system, the domination of interfacial tension and inertial force leads to various interfaces in regular shapes (Plutschack et al., 2017). There are many types of liquid-liquid flow patterns on a micro-scale. The main flow patterns observed in silicone and Teflon microchannels are annular, slug, and droplet flow (Tsaoulidis et al., 2013), but among the flow patterns, slug flow is ideal for enhancing mass and heat transfer due to the high stability characteristics shown by this flow pattern, and its ability to

E-mail address: aloy_sius_yw@staff.ubaya.ac.id (A.Y. Widianto).

^{*} Correspondent author.

Nomenclature		Greek 1	Letters
a specific su Ai interfacial C concentrat Ca Capillary r D diameter, Ei enhancem K overall ma k mass trans Q volumetric Re Reynolds r	ion, mol/liter number m diffusivity, m²/s ent factor for instantaneous reaction ss transfer coefficient, m/s fer coefficient of the film, m/s flow rate, m³/s number ite, mol/liter/s city, m/s	τ ρ μ σ Subscri A B c d org aqu o Superso	reaction time, s fluid density, kg/m³ fluid viscosity, Pa s or kg/m/s surface tension, kg/s² ipts species of CCl ₃ COOH species of Sodium Hydroxide solution organic phase aqueous phase organic phase aqueous phase initial condition

generate a substantial specific surface. Annular flow appears while inertial force works more dominant than interfacial tension force. Interfacial tension force tends to reduce interfacial area, whereas inertial force breaks the shape and drags the interface in the flow direction. As the competitive nature between inertial and interfacial tension forces, annular flow can be destabilized by changing the flow rate of both phases and the flow rate ratio. Slug and droplet flows are extensively studied because of the ease of hydrodynamic control and potential applications in fine chemical synthesis. Operations in the slug flow regime have been demonstrated to become a valuable tool for increasing reaction performance limited by mass and heat transfer. Furthermore, the ease of slug dimensions control allows a more effective mass transfer process and reaction control, which is unachievable in batch and continuous stirred tank reactors (Ratchananusorn et al., 2011). In this case, two mechanisms are found to be responsible for mass transfer between liquid-liquid two-phase flow: first, internal circulations within the slug; second, gradient concentration between successive slugs leads to diffusion between phases. With its advantages, microfluidic systems are employed for increasing mass and heat transfer in many industrial purposes, such as the dehydration of bioethanol (Suerz et al., 2021), synthesis of ethyl methyl oxalate from diethyl oxalate (Ji et al., 2020), Biodiesel synthesis through transesterification (Wu et al., 2016; Tiwari et al., 2018; Mazubert, 2014; Jamil et al., 2016), fabrication of wrinkled protein microcapsules (Feng and Lee, 2019), and generation of gelatin emulsions and microcapsules (Yeh et al., 2013).

Compared to conventional systems, microdevices offer other advantages, such as effective mixing processes and process safety, mainly for processes employing hazardous and toxic chemicals such as nitration and polymerization. However, the microreactor performance still needs improvements, considering the potential occurrence of fouling in some chemical process applications due to chemical degradation, which is difficult to detect and clean because of the small diameter of the channel. The emergence of this problem will undoubtedly be troublesome when the scale-up process is carried out. Therefore, more in-depth and comprehensive studies regarding the scale-up process toward industrial capacity are still urgently needed (Jensen, 2017).

Flow behavior greatly determines the sustainability of the mass and heat transfer processes on the micro-scale. Mass transfer characteristics on a micro-scale differ from those on a macro-scale, mainly related to thin liquid film formation in a narrow space between the slug and channel wall and the diffusion process between phases. On a micro-scale, liquid films emerge in a more delicate dimension. Hence, the distance of molecular diffusion on a micro-scale becomes shorter and increases the mass transfer coefficient significantly. Some previous researchers have worked on the mass transfer phenomena in

microreactors. What distinguishes the current study from previous studies is the channel cross-section, channel material, and the liquid phase used. Previous studies employed channels with square (Dessimoz et al., 2008) and triangular cross-sections (Basher, 2021), while this study utilized circular cross-sections. The effect of channel materials was observed using glass tube (Dessimoz et al., 2008), PTFE (polytetrafluoroethylene) (Ghaini et al., 2010; Xu et al., 2013), PMMA (Kovalev and Yagodnitsyna, 2021), and PFA (Wang et al., 2020), while this study employed two different channel materials, i.e., silicone and PTFE. Sodium hydroxide-NBF ester was used as a liquid-liquid mixture (Ghaini et al., 2010), whereas the current study uses the liquid mixture of water-NaOH and CCl₃COOH-toluene as aqueous and organic phases. The tube cross-section, channel material, and different physical properties of the liquid determine the characteristics of the slug flow pattern generated. The various contact angles and liquid wettability on a channel wall affect the overall mass transfer coefficient (Wang et al., 2020; Liu et al., 2021; Antony et al., 2014).

The studies on mass transfer phenomena in microfluidic systems have been widely published (Zhang et al., 2019; Ratchananusorn et al., 2011; Wang et al., 2020; Liu et al., 2021; Zhang et al., 2012), but the previous results did not explain the correlation between slug dimensions and the mass transfer coefficient. In addition, previous studies have yet to study the impact of various channel materials on the mass transfer process between phases. Therefore, this work focused on exploring the liquid-liquid mass transfer phenomena regarding slug flow pattern and the influence of slug dimensions, channel material, volumetric flow rate, and the organic-to-aqueous flow rate ratio on the mass transfer coefficient.

2. Materials and methods

2.1. Material

The hydrodynamic of two-phase microfluidic systems has three different aspects to be considered: the first, the surface area to volume ratio; the second, the flow was characterized by a small Capillary number (C_a), which expresses that the influence of surface tension force is more predominant than viscous force in the system; and the third, micro-roughness and wettability channel wall exert significant influence to the formation of flow pattern. The two-phase flow pattern observed in the experiment consists of an aqueous and an organic phase. The aqueous phase involved a mixture of deionized water and NaOH (Fisher Scientific, ≥ 98 %) with 0.1, 0.13, and 0.15 M concentration, and the organic phase comprised a mixture of toluene (Merck, ≥ 99.9 %) and CCl₃COOH (strong acid) (Sigma Aldrich, ≥ 99 %) with the concentration

of 0.4 M. Then, bromothymol blue was used as an indicator to facilitate flow observations. The physical properties of aqueous and organic phases at 25 $^{\circ}$ C are depicted in Table 1 below:

2.2. Equipment

The microchannel in this work has a 1 mm inside diameter and 15 cm long of PTFE and silicone materials. Two syringe pumps (NEM-ESYS high-pressure syringe pump type NEM-B203–01 B) were applied to ensure the stability of liquid flow along the channel. This pump can flow liquid with minimum and maximum debits in the range of 171.0 nl/min – 825 ml/min, maximum pumping pressure of 12 bar for 100 ml syringe, and liquid discharge in the field of 42.7 nl/min – 206 ml/min with a maximum pumping pressure of around 50 bar for a 25 ml syringe.

Visualization of the two-phase flow pattern was carried out by using a High-Speed Digital Camera (CCD HCC-1000) and an SMZ-10 microscope (Nikon) using image processing software NV 1000 (New Vision Technologies) and a light source (LED lamp), allowing slug shape and color changes detection to be observed clearly.

2.3. Method (continuous)

Principally, the experiment was carried out in three stages, i.e., slug formation in a microchannel, then visualizing slug flow pattern and measuring the slug length within a channel. Measuring slug length was conducted using a method depicted in Fig. 2. The ruler in Fig. 2 only intends to clarify the principle of the applied method. All measurements were conducted using the image processing software NV 1000 at ambient temperature and pressure (Figs. 1 and 3).

2.4. Analysis

To determine the overall mass transfer coefficient, neutralization was used as a reaction model with color change at pH 7 by bromothymol blue as an indicator. The reaction is instantaneous, thereby, controlled by mass transfer. The neutralization reaction takes place between ${\rm CCl_3COOH}$ and NaOH according to the stoichiometry as follows:

$$CCl_3COOH + NaOH \rightarrow CCl_3COONa + H_2O$$
 (1)

The reaction rate is expressed for the strong acid component ${\rm CCl_3COOH}$,

$$\frac{dN_{A,org}}{dt} = V_{A,org} \cdot \frac{dC_{A,org}}{dt} = -A_i \cdot K_L \cdot \left(C_{A,org} - C_{A,org}^* \right)$$
 (2)

 $N_{A,org}$ represents CCl₃COOH in the organic phase, while A_i is the interfacial area of two liquid phases. Eq. (2) can be expressed in another form by defining the holdup of the organic phase,

$$\varphi_{A,org} = \frac{V_{A,org}}{V_{mc}} = \frac{Q_{A,org}}{Q_{A,org} + Q_{A,aau}} = \frac{1}{1+q}$$
(3)

$$q = \frac{Q_{A,aqu}}{Q_{A,org}} \tag{4}$$

where Q_{org} and Q_{aqu} are the volumetric flow rates of the organic and aqueous phases, respectively. Then, specific surface,

Table 1Physical properties of aqueous and organic phases.

Fluids	ρ (kg/m ³)	$\mu (kg/m.s).10^3$	σ (N/m)	
1141415	p (16/111)	μ (1.8) 1110)110	0 (11, 111)	
NaOH	2130	-	-	
CCl ₃ COOH	1630	-	-	
Toluene	887	0.5600	0.02785	
Water	997	0.8937	0.07180	

 $\rho=$ density, $\mu=$ viscosity, $\sigma=$ surface tension (Melo-Espinosa et al., 2014).

$$a = \frac{A_i}{V_{mc}} \tag{5}$$

By substituting Eqs. (3) - (5) into Eq. (2), the following equation will be obtained:

$$\varphi_{A,org} \frac{dC_{A,org}}{dt} = -a.K_L. \left(C_{A,org} - C_{A,org}^* \right)$$
 (6)

with K_L as the overall mass transfer coefficient. Because NaOH instantly neutralizes the CCl₃COOH molecule transferred to the aqueous phase close to the interface, the concentration of CCl₃COOH in the aqueous phase ($C_{A,aqu}$) can be assumed to be zero, so $C_{A,org}^* = \text{m.} C_{A,aqu}^* = 0$.

$$\varphi_{A,org} \frac{dC_{A,org}}{dt} = -a.K_L.C_{A,org} \tag{6}$$

By integrating Eq. (6), the following volumetric mass transfer coefficient equation will be obtained:

$$K_L.a = \frac{\varphi_{A,org}}{\tau}.\ln\left(\frac{C_{A,org}^0}{C_{A,org}^\tau}\right) = \frac{1}{\tau.(1+q)}.\ln\left(\frac{C_{A,org}^0}{C_{A,org}^\tau}\right)$$
(7)

$$\tau = \frac{A_{mc} \cdot L_{\tau}}{Q_{A,org}} \text{ and } C_{A,org}^{\tau} = C_{A,org}^{0} - q \cdot C_{B,aqu}^{0}$$
(8)

au is the time required for a complete neutralization reaction. Eq. (7) was used to calculate the volumetric mass transfer coefficient of liquid-liquid two-phase flow in a microchannel.

3. Results and discussion

The hydrodynamics were studied in 1 mm inside diameter using PTFE and silicone tubes at various sodium hydroxide concentrations and the organic-aqueous flow rate ratios at various total flow rates ($Q_d + Q_c$) in the range of 30 – 40 ml/h. Among the liquid-liquid flow patterns that may be formed, slug flow exhibits the most stable characteristics. It has good potential for industrial applications involving mass and or heat transfer. Therefore, this study observed slug flow patterns focusing on mass transfer in microchannels with T-junction.

3.1. Liquid-liquid two phases flow pattern within a microreactor

Droplet, slug, and annular flow patterns were observed in the current study using circular channels. The flow pattern generated in a microfluidic system is greatly influenced by several factors, i.e., physical properties of fluid such as density, viscosity, surface tension, and contact angle. Channel diameter, material used, and experimental conditions such as pressure, temperature, and flow rate. Changes in channel shape and dimensions affect fluid flow, resulting in different flow patterns. The channel shapes often used in microfluidic systems are square, circular, and triangular under very fine diameters. However, the current experiment observed the mass transfer performance using a circular channel with a 1 mm inside diameter. On a micro-scale, the influence of gravitational forces becomes reduced; conversely, the performance of inertial, capillary, and surface tension forces becomes dominant and determines the formation of flow patterns. The dominance of each force can be sorted by determining dimensionless numbers (Reynolds, Capillary, and Weber numbers) because the magnitude of these numbers was affected by the performance of these forces. At constant temperature, the inertial force is primarily affected by the flow rate of the organic and aqueous phases. In contrast, the viscous force and surface tension are strongly determined by liquid density and viscosity. The density and viscosity will change at different concentrations. Changes in density and viscosity are more affected by the sodium hydroxide concentration than temperature because the operating temperature in this work was kept constant.

The droplet flow pattern was obtained when the flow rate of the

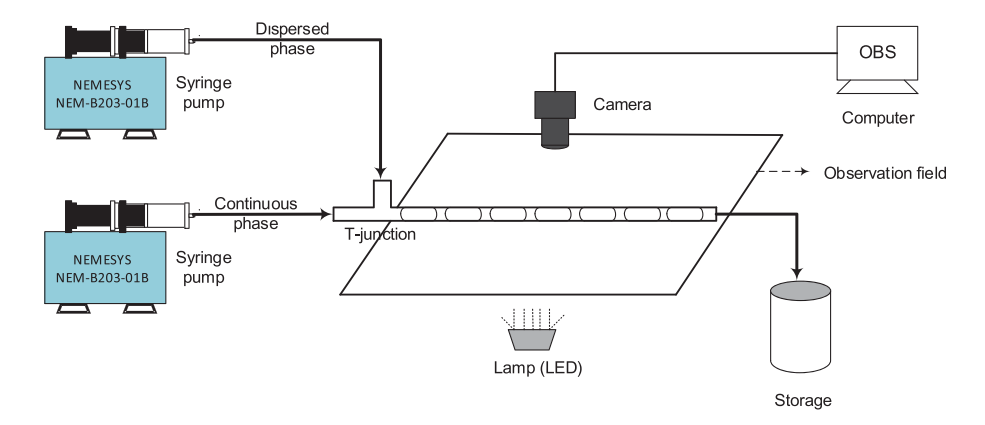


Fig. 1. Experimental setup.

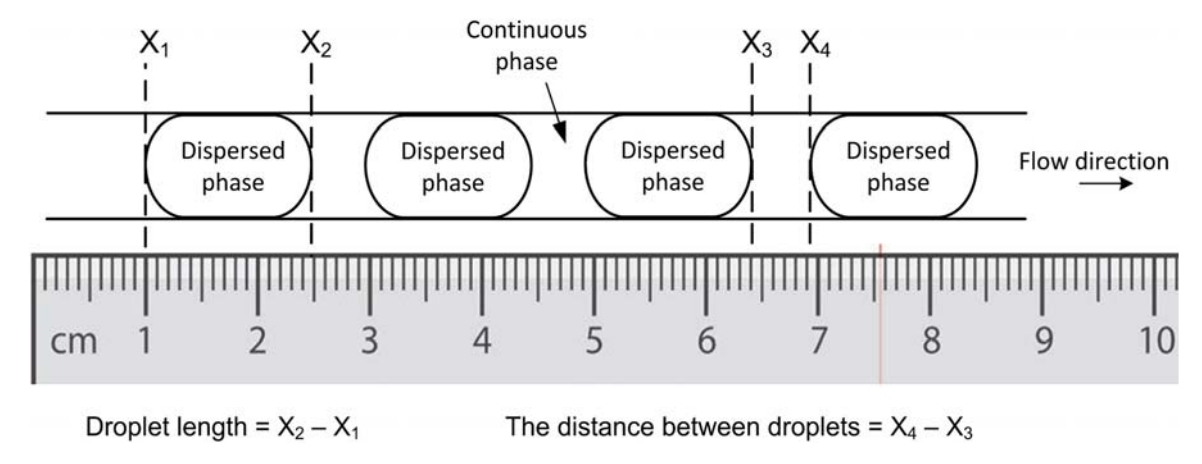
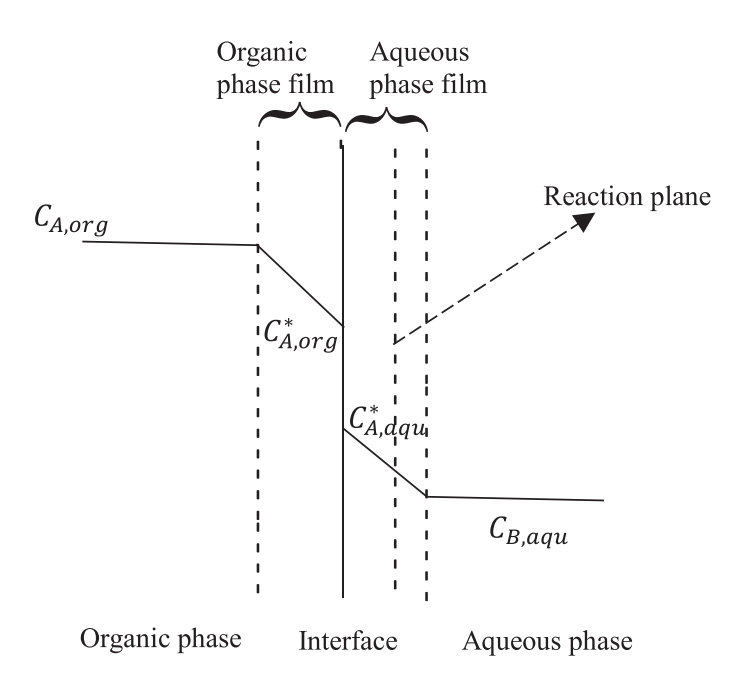


Fig. 2. The measuring method of droplet dimension and the distance between droplets. The horizontal positions of X_2 and X_1 indicate the droplet length, and the different positions of X_4 and X_3 show the distance between the droplets.



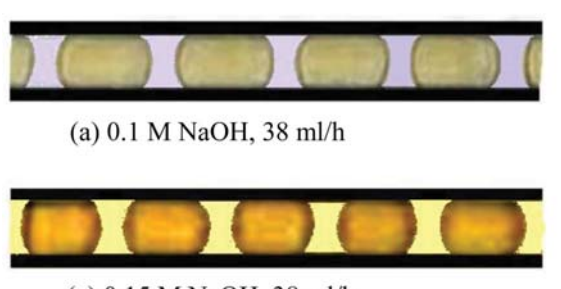
 $\textbf{Fig. 3.} \ \ \text{Mass transfer mechanism between phases.}$

organic phase was too low compared to the aqueous phase, with a ratio of less than 0.6. Droplets appeared under a diameter smaller than the inner diameter of the channel. Meanwhile, an annular flow pattern emerged over a more substantial flow rate ratio of the organic-to-aqueous phase, i.e., more than 1.1. The slug flow pattern, which is the focus of the current study, was generated when the flow rate ratio of the organic to aqueous phases was 0.6-1.1 for both PTFE and silicon channels. The slug flow pattern emerged when the surface tension dominated inertial and viscous forces.

Fig. 4(a)–(d) present the slug flow pattern observed in the microchannel. Sodium Hydroxide solution in the flow system formed droplets with a length over 1 mm dispersed in CCl_3COOH -toluene with a standard deviation below 12 % at the longest slug generated by the lowest sodium hydroxide concentration. At a total flow rate over 40 ml/h for the lowest sodium concentration (0.1 M), slug flow became unstable, indicated by the slug dimension emerging from 3 to several mm long. The slug length remained relatively constant for the total flow rate between 30 and 40 ml/h, with the dimensionless number presented in Table 3.

Slug flow observations using a high-speed camera have not detected any thin liquid films formed between droplets and channel walls. The outer surface of the dispersed phase is in direct contact with the channel wall. CCl₃COOH-toluene in both channels has much smaller contact angles than sodium hydroxide solutions. Therefore, CCl₃COOH-toluene has better wetting properties than sodium hydroxide solutions and is strengthened by the nature of immiscible liquids, causing the volume of the continuous phase in the narrow space between slug and channel walls to become very small because the continuous liquid will tend to be drawn out of this zone. The release of the liquid continuous from the narrow space caused the droplets of sodium hydroxide to come into direct contact with the channel walls. The measurement results of the contact angles of sodium hydroxide solutions and CCl₃COOH-toluene are presented in Table 2.

In a specific chemical process involving mass transfer, the presence of a thin liquid film in the narrow space between droplets and channel walls is advantageous. The formation of a thin liquid film will enhance the specific surface area, i.e., the ratio between surface area and volume of droplets, which is required for effective mass transfer between phases. In a thin liquid film, the mass transfer occurs at the interface between the organic and aqueous phases across the entire surface of the droplet. Conversely, if a thin liquid film does not appear within a flow system, the mass transfer will only occur at the interface of the head and tail of the droplets. In the current work, CCl₃COOH in the CCl₃COOH-toluene mixture diffused from organic to aqueous phases. The mass transfer occurred in one direction towards the aqueous phase because the sodium hydroxide solution did not diffuse toward the CCl3COOH-toluene mixture. Furthermore, a neutralization reaction occurred between CCl₃COOH and sodium hydroxide solution with a high reaction rate at the aqueous phase interface. The reaction led to a color change from blue to yellow in the aqueous phase, which takes place at pH 7, indicating the end of neutralization.



(c) 0.15 M NaOH, 38 ml/h

Table 2The various contact angles of liquid mixtures in the PTFE and silicone channel.

Components	Contact Angles	
	PTFE	Silicone
Sodium Hydroxide solution (0.1 M)	91°	56°
Sodium Hydroxide solution (0.15 M)	92°	59°
CCl ₃ COOH-toluene (0.4 M)	12°	5°

Table 3Dimensionless Numbers for slug flow observed.

Dimensionless Numbers					
Reynolds number organic phase, $(R_{e,d})$ Reynolds number aqueous phase, $(R_{e,c})$	inertial forces viscous forces	$R_{e,d} = rac{D.v_d. ho_d}{\mu_d}$ Christie and Geankoplish (1993) $R_{e,c} = rac{D.v_c. ho_c}{\mu_c}$ Christie and Geankoplish	1.3117-1.7489 0.0755-0.1006		
Capillary number, (C_a) Weber number, (W_e)	viscous forces surface tension forces inertial forces surface tension forces	(1993) $C_a = \frac{\mu \cdot \nu}{\sigma} \text{ Volkel}$ et al., (2008) $W_e = \frac{\nu^2 \cdot D \cdot \rho}{\sigma} \text{ Volkel}$	0.00375-0.1143		
		et al., (2008)			

3.2. Dimensionless number

The Reynolds, Capillary, and Weber numbers are three important dimensionless numbers in the study of fluid flow. A comprehensive analysis of the dimensionless numbers was conducted to get an overview of slug formation within microchannels because, from these numbers, the predominant forces working in the microsystem can be identified.

Table 2 presents that the Reynolds number (R_e) of the organic phase is over one in the range 1.3117-1.7489, while the Reynolds number of the aqueous phase is less than one in the field 0.0755-0.1006. These values indicate that inertia force gave a more dominant influence than viscous force in the organic phase, and vice versa; viscous force has a more dominant effect than inertial force in the aqueous phase. The slightly different results exhibited by the Capillary number in these observations. The magnitude of the Capillary number (C_a) is less than one for both phases in the range of 0.00375-0.1143. These values characterized that in this flow system, surface tension exerts a more dominant influence in the organic and aqueous phases than viscous forces. A similar trend is described by Weber's number of the organic and aqueous phases, which exhibits a value of less than one in the range of 0.0049 - 0.0115. Weber number of less than one expresses that surface tension significantly influences organic and aqueous phases more than inertial forces. Knowing the predominant force working on each phase facilitates determining the flow rate ratio of the organic to

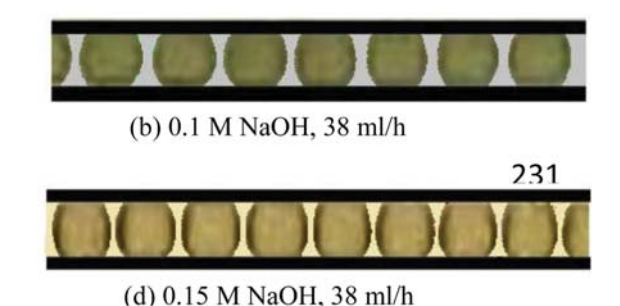


Fig. 4. (a) (c) Slug flow pattern within PTFE tube, (b) (d) within Silicone tube.

aqueous phases on slug flow generation (Yao et al., 2018).

For the organic phase, the predominant force in order from the largest to smallest is as follows: surface tension, inertial, and the smallest one is viscous force. In the same manner, the dominance force in order from the largest to smallest one for the aqueous phase is as follows: surface tension, viscous force, and minor inertia force. The influence of inertial forces increased with increasing fluid linear velocity of ρU^2 (U =fluid velocity). Furthermore, increasing fluid velocity bring to increasing the viscous forces affect on the liquid-liquid systems with a linear correlation at a specific viscosity, $\mu U/l$ (where $\mu =$ fluid viscosity; l = length characteristic). Then, if these forces are compared, the inertial force denotes a more considerable increase, which means that increasing the volumetric flow rate increases the Reynolds number significantly (see Fig. 5). As the flow rate ratio of the organic-aqueous phase grew, the dimensions of the slug appearing within the channel increased along with this ratio. A continuous enhancement of this ratio will be followed by an increase in slug dimension, eventually transitioning toward an annular flow pattern. Conversely, decreasing this ratio transforms slug to droplet flow, which is gradually less stable. Apart from viscous and inertial forces, surface tension forces also contribute to the slug length within the channel. Increasing interfacial tension force is favorable for slug formation, but a decreasing interfacial tension force tends to produce parallel flow in a microfluidic system. In industrial processes, the low stability behavior is undesirable because, under the low stability of processes, it will be difficult for an engineer to estimate many things related to process behavior, such as reaction conversion achievements, yields, production capacity, etc. Therefore, slug formation is more desirable and studied related to mass transfer in a microsystem. The slug formation with the smallest dimension and high stability is needed to generate a large specific surface area for effective mass transfer between phases.

The correlation of Reynolds number to Capillary and Weber number is denoted in Fig. 5. This figure also obviously exhibits the influence of inertial, viscous, and surface tension forces on microfluidic systems. The correlation curve of Reynolds number and Weber number provides information that the increase in Reynolds number due to an increase in inertial force is in line with the increase in the Weber number, shown on the vertical axis. Increasing the Weber number explicitly expresses that the influence of inertia force relative to the surface tension force will be greater. The correlation curve of the Reynolds number and Capillary number indicates the same trend. Enhancing Reynolds number is

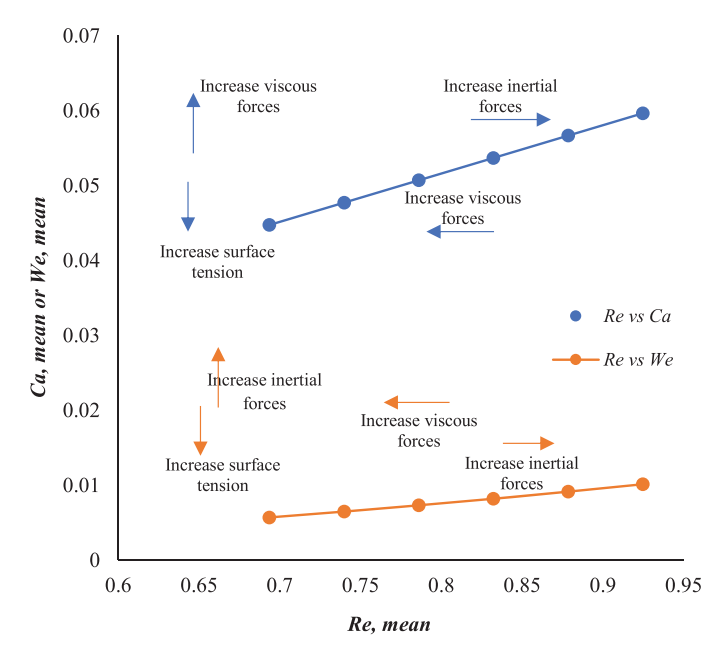


Fig. 5. The correlation between dimensionless numbers in the slug regime.

followed by an increase in Capillary number, which means that the viscous forces have a more considerable influence relative to surface tension forces.

3.3. Overall mass transfer coefficient

The volumetric mass transfer coefficient was determined using Eq. (7). Fig. 6(a)(b) depicts that the greater the total flow rate for the constant organic discharge, the greater the volumetric mass transfer coefficient obtained. These results indicate a similar trend to work conducted by Xu et al. (2013) (Zhang et al., 2019) and Wang et al. (2020) (Plutschack et al., 2017), which is, in this total discharge, T-junction will generate a smaller slug dimension with a more significant number of droplets appeared in the same channel length. The various flow rate ratios of the organic-aqueous phase were found to be an effective method for slug dimensions control. The increase in these ratios has led to an upward trend in the slug dimensions of the organic phase and a downward trend in the distance of successive slugs. The tiny dimension can provide a larger specific surface area (A/V) than the longer slug in a given channel length. The continuous increase in specific surface area brings up the higher volumetric mass transfer coefficient. Therefore, if the curves in Fig. 6(a) and (b) are compared, the volumetric mass transfer coefficient obtained on the tube with silicone material is higher than that for PTFE. This result aligned with the graphs in Figs. 8 and 9(a) and the trend of flow dimensions as illustrated in Fig. 4(a)-(d). These images present that the slug dimensions in PTFE have a longer dimension than the silicone channel (Fig. 7).

The concentration of the aqueous phase, sodium hydroxide, also determines the mass transfer coefficient. The utilization of a higher sodium hydroxide concentration ($C_{B,aqu0}$) with a constant organic phase concentration has enhanced the volumetric mass transfer coefficient (see Fig. 6(a) and (b)). Under these conditions, the final concentration of CCl_3COOH in the organic phase is getting smaller ($C_{A,org}$) since more CCl_3COOH is involved in neutralizing NaOH (Eqs. (1) and (2)). The reaction occurred in the aqueous phase interface because the sodium hydroxide solution could not diffuse into the organic phase. Conversely, CCl_3COOH in the organic phase is able to diffuse (Xu et al., 2013) in the aqueous phase and dissolve in water. The occurrence of neutralization is indicated by a color change from blue to yellow in the aqueous phase, where the presence of yellow in the flow system denotes that the neutralization has been completed.

The influence of sodium hydroxide concentration on the mass transfer coefficient has been described by previous researchers (Xu et al., 2013; Dessimoz et al., 2008). From different points of view, they explained that the mass transfer coefficient increased due to the increasing sodium hydroxide concentration. This correlation is approached by the effect of sodium hydroxide concentration on the slug dimensions. As the aqueous phase's linear velocity (U_c) exceeds the organic phase (U_d) , the slug had small sizes and generated a large specific surface area and a high volumetric mass transfer coefficient. These explanations will be relevant for some cases with large sodium hydroxide concentrations. Nevertheless, for the cases with moderate sodium hydroxide concentration, the change in liquid viscosity caused by changes in sodium hydroxide concentration in the mixture was insignificant (Yao et al., 2020). Hence, the chosen approach needs to be more precise in this situation. The profile of slug dimensions with variations in sodium hydroxide concentration is depicted in Figs. 8 and 9(a). The trend indicates that sodium hydroxide concentration is inversely proportional to the slug dimensions in the channel. The microchannel will generate the largest slug dimensions at the minor sodium hydroxide concentration. In this case, a smaller viscosity of the aqueous phase creates a lower hydrodynamic resistance. The lower hydrodynamic resistances and trend of inertial force to drag downstream surfaces were responsible for higher slug dimensions in a microflow system.

Fig. 7 describes the correlation of the volumetric mass transfer coefficient in a PTFE and silicone tube with various sodium hydroxide

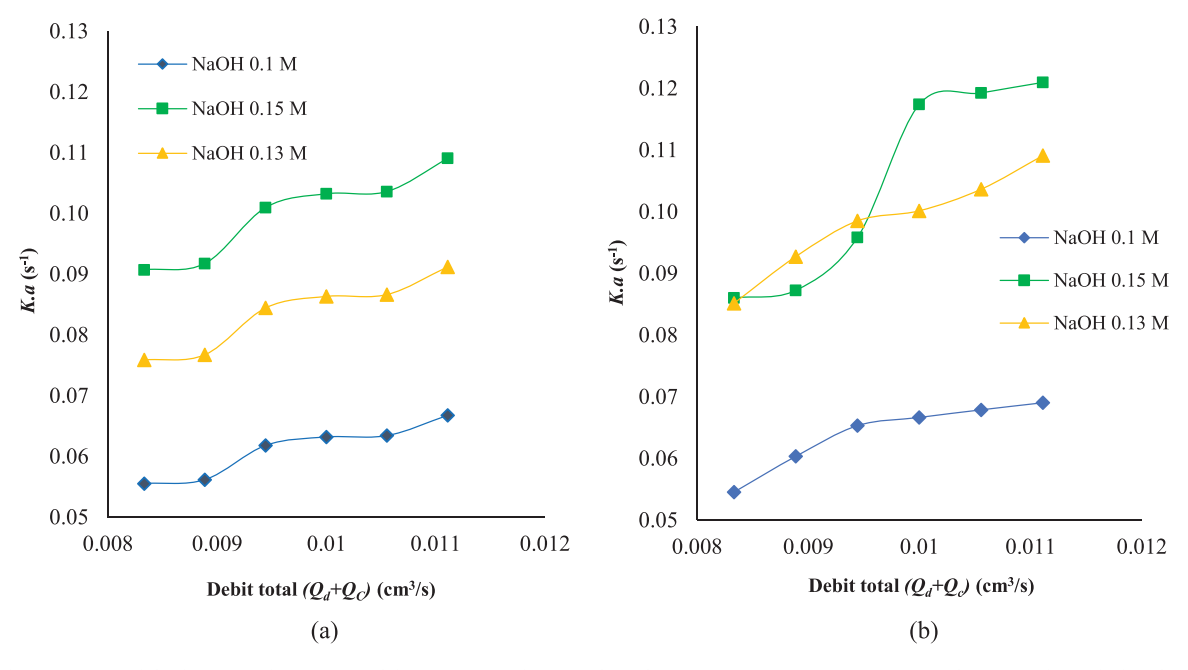


Fig. 6. (a) The effect of total discharge (with a constant debit of organic phase) to the volumetric mass transfer coefficient within PTFE channel, (b) Silicone channel.

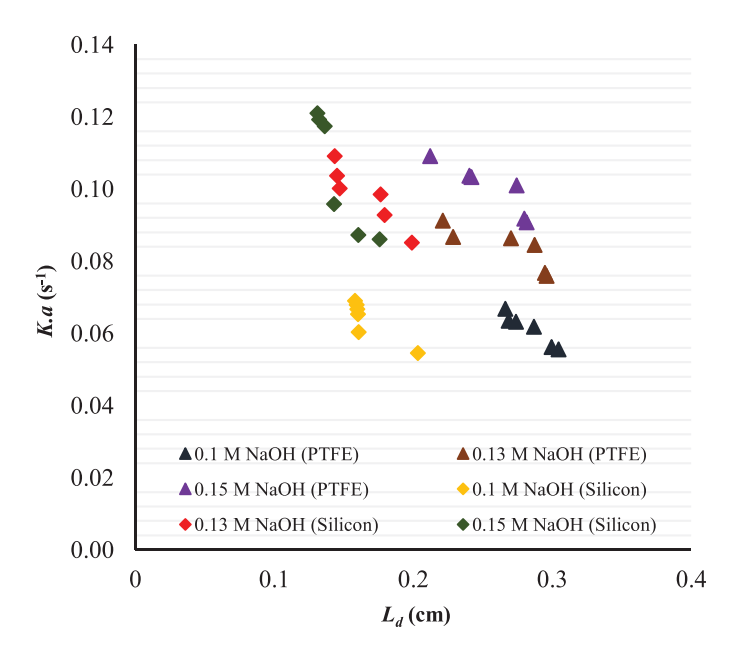
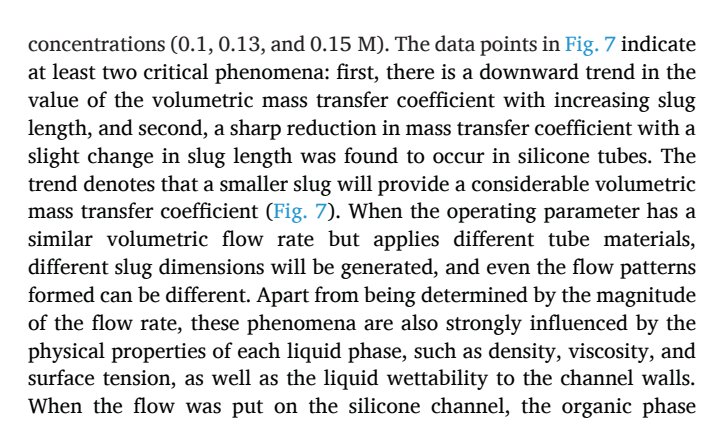


Fig. 7. The correlation between droplet length (L_d) and the volumetric mass transfer coefficient K.a.



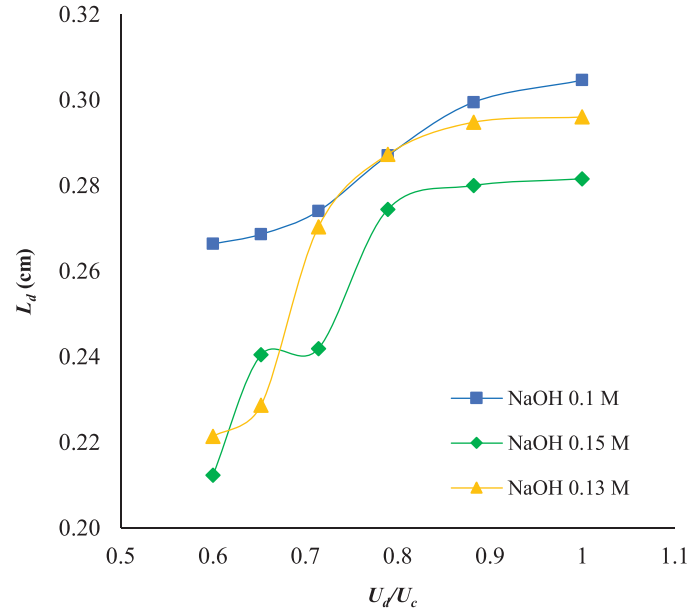


Fig. 8. The organic-to-aqueous phase linear velocity ratio (U_d/U_c) influences the droplet length (L_d) in the PTFE channel.

thoroughly wets the channel wall with a tiny contact angle (Prakash and Ghosh, 2021). In contrast, the organic phase forms a larger contact angle in the PTFE channel, indicating that it possesses poorer wetting properties than silicone. At a certain level, this flow behavior triggers the generation of different flow patterns.

From the experiments, the highest volumetric mass transfer coefficient obtained is 0.121/s, with a mass transfer rate of 0.0182 M/s. These values were at a concentration of 0.15 M NaOH with the rate of the organic and aqueous phase of 15 ml/hour and 25 ml/hour, respectively (total volumetric flow rate is 40 ml/hour), and this result was attained by using the silicone channel. The calculation assumes the slug shape is a cylinder with a hemispherical front and rear cap.

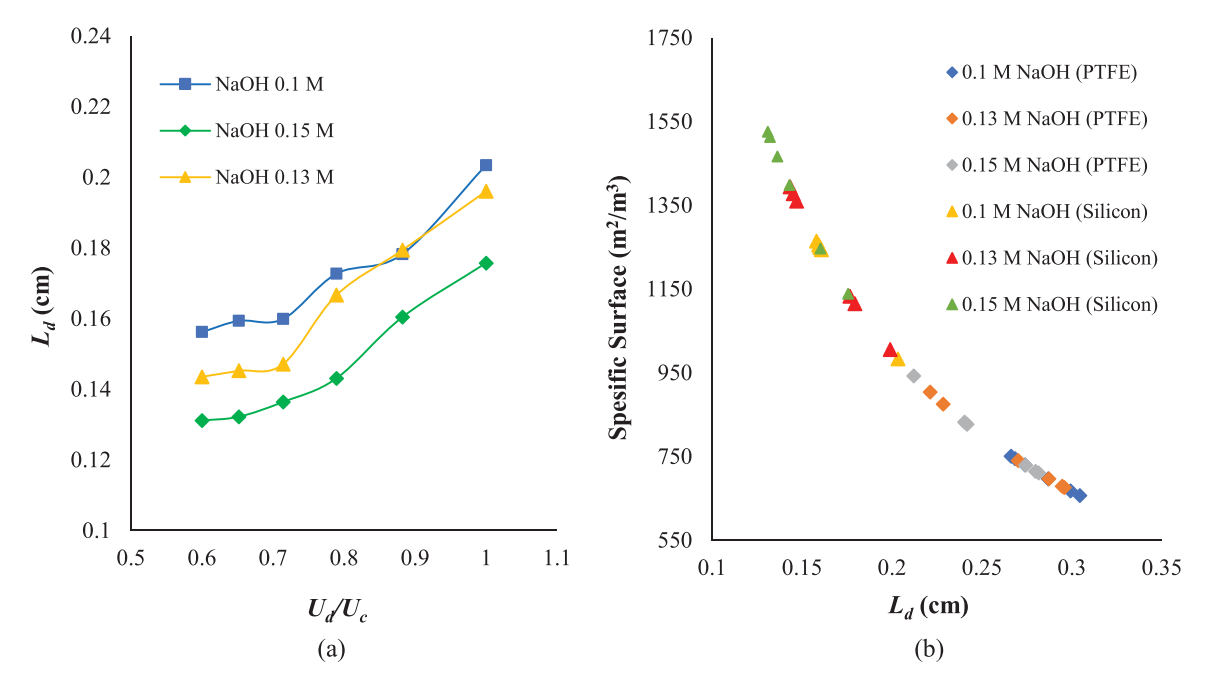


Fig. 9. (a) The effect of the organic-to-aqueous phase linear velocity ratio (U_d/U_c) on the droplet length in the silicone channel, (b) The correlation between droplet length (L_d) to the specific surface area on PTFE and silicone channels.

3.4. Mass transfer model under liquid-liquid slug flow

The mass transfer model under the slug flow pattern can be explained through two distinct mechanisms: i) the diffusion over the interface of both phases and ii) convection by internal circulation. Both mechanisms take place simultaneously with the different dominance of diffusion and convection depending on operating parameters. An increase in the linear velocity of the organic phase as a continuous phase leads to a decrease in the slug length, creating a larger interfacial area and significantly impacting diffusion between phases. Furthermore, the increasing linear velocity also increased internal circulation within the slug's body, enhancing mass transfer by convection.

If the mass transfer occurs via diffusion, the model can be derived by considering a stagnant microflow system. The detailed phenomena were explained by considering neutralization steps between CCl $_3$ COOH and sodium hydroxide solution. Neutralizing sodium hydroxide solution with CCl $_3$ COOH is an instantaneous reaction with the reaction plane located at the liquid film's aqueous phase. The reaction is controlled by the mass transfer of CCl $_3$ COOH and sodium hydroxide solution. All CCl $_3$ COOH compounds have run out at the reaction plane. It means no CCl $_3$ COOH diffused to the bulk of the sodium hydroxide solution.

Changes in CCl₃COOH and sodium hydroxide concentrations will shift the reaction plane. At a steady state, the flow rate of sodium hydroxide toward the reaction zone is equal to the flow rate of CCl₃COOH toward the reaction zone (Fig. 10). Thus,

$$-r'_{A,org} = -r'_{B,qu} = k_{A,org} \left(C_{A,org} - C^*_{A,org} \right) = k'_{A,org} (C^*_{A,aqu} - 0) \cdot \frac{X_0}{X}$$

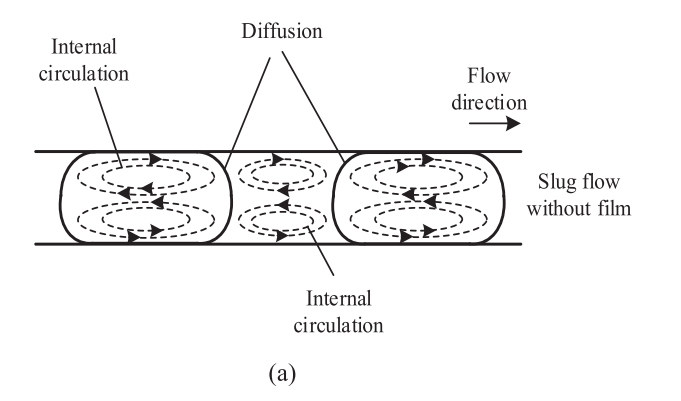
$$= k_{B,aqu} \left(C_{B,aqu} - 0 \right) \cdot \frac{X_0}{X_0 - X}$$
(9)

Where $k_{A,org}$, $k_{A,aqu}$, $k_{B,aqu}$ is the mass transfer coefficient of CCl₃COOH in the organic phase, aqueous phase, and mass transfer coefficient of sodium hydroxide in the aqueous phase, respectively, thereby, the mass transfer coefficient within the film correlates,

$$\frac{k_{A,aqu}}{k_{B,aqu}} = \frac{D_{A,aqu}/X_0}{D_{B,aqu}/X_0} = \frac{D_{A,aqu}}{D_{B,aqu}}$$
(10)

$$\frac{1}{K_{A,org}} = \frac{1}{k_{A,org}} + \frac{m}{k_{A,aqu,E_i}}$$
(Hatta Theory) (11)

If the system uses pure reactant CCl₃COOH, then $C_{A.org} = C_{A.org}^*$. Another mechanism that accompanied the mass transfer diffusion in



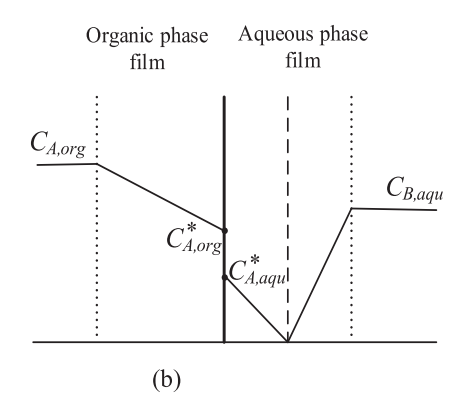


Fig. 10. (a) Mass transfer mechanisms (diffusion & convection) within slug flow, (b) Interface behavior for neutralization (Wang et al., 2017).

the microfluidic observed was convection by internal circulation. Convective mass transfer involves transferring materials between a liquid surface and a moving fluid or between CCl₃COOH-Toluene and sodium hydroxide solution that is relatively immiscible. The convective mass transfer took place under the influence of syringe pump performance. In this system, there was no density variation for both organic and aqueous phases because the temperature parameters remained constant during the flow observation, and the sodium hydroxide concentrations were relatively low. However, it should be noted that the influence of fluid density cannot be ignored at a higher concentration of sodium hydroxide. The transfer rate equation is reliable by

$$N_A = k_c \cdot (C_{AS} - C_A) \tag{12}$$

where N_A is the molar mass flux of CCl₃COOH species measured relatively to the fixed spatial coordinates; k_c is the convective mass transfer coefficient; C_{AS} is the concentration at the boundary layer; and C_A is the concentration at some arbitrary defined point in CCl₃COOH-Toluene. The mass transfer coefficient is related to the fluid properties, the hydrodynamic characteristics of the fluid, and the geometry of the preferred system.

The influence of internal circulating flow on mass transfer performance in slug flow can be explained using surface renewal theory. The theory developed by Danckwerts applies penetration theory, where the liquid is described as two areas, i.e., a well-mixed bulk area and an interfacial area, which is renewed so quickly, thus making this area behave like a thick film, as seen in Fig. 11. The dynamic nature of the liquid-liquid interfaces is the principal characteristic of this theory. The assumptions used in this theory are (1) the liquid components at the interface change randomly with fresh components from the well-mixed bulk area; (2) at any time, each liquid component at the interface has the same opportunity to be replaced by a new liquid component; and (3). mass transfer from one liquid to another occurs at the interface under unsteady state conditions. Therefore, the difference in liquid volume at the liquid-liquid interface is renewal due to turbulence around the interface, which is called surface renewal frequency (S).

For a liquid-liquid system like in the current work with the mass transfer taking place from liquid A to B, surface renewal theory states that the mass transfer coefficient on liquid A and B sides are in the surface renewal frequency (S) and molecular diffusivity of liquid A

toward B according (D_{AB}) to the following equation:

$$k_L = (D_{AB}.S)^{0.5}$$
 (9)

Eq. (9) obviously shows that an increase in surface renewal frequency (S) due to an increase in internal flow velocity in the slug flow at the liquid-liquid interfacial area will increase the mass transfer performance (k_L). The figure below exhibits a model of mass transfer phenomena between NaOH-water (aqueous phase) and CCl₃COOH-toluene (organic phase). The reaction occurred in the aqueous phase interface because the Sodium hydroxide solution could not diffuse into the organic phase. Conversely, CCl₃COOH in the organic phase is able to diffuse in the aqueous phase and dissolve in water.

4. Conclusions

Slug flow patterns were observed in the PTFE and silicone channels. In the microsystem, the gravitational force did not influence the flow formation. In the observed system, surface tension, inertial, and viscous force were the predominant forces influencing the flow system. Sodium hydroxide solution as an aqueous (dispersed) phase and CCl3COOHtoluene as an organic (continuous) phase have better wettability in the silicone channel than the PTFE channels. The wettability of the sodium hydroxide solution on the channel wall determines the shape of the head and tail of the slug and the dimension. The slug on the PTFE channel indicates a more rounded head and tail shape with a larger contact angle. Channel material is one factor that influences the formation of flow patterns. In terms of operating conditions, using a higher total discharge, mainly for the volumetric flow rate of the aqueous phase lower than the organic phase, the microfluidic system will generate a smaller slug dimension and a larger specific surface area (A/V). A substantial specific surface area (A/V) will facilitate an upward trend on the volumetric mass transfer coefficient. The concentration of sodium hydroxide solution was also found to determine the slug dimensions. The trend exhibits that enhancing the sodium hydroxide concentrations decreases slug dimensions. In the current work, the highest distinctive character (A/V) is 100,282.563 m²/m³ with a volumetric mass transfer coefficient of 0.121/s and a mass transfer rate of 0.0182 M/s. This value was reached at a sodium hydroxide concentration of 0.15 M, an organic flow rate of 15 ml/hour, an aqueous flow rate of 25 ml/hour (total

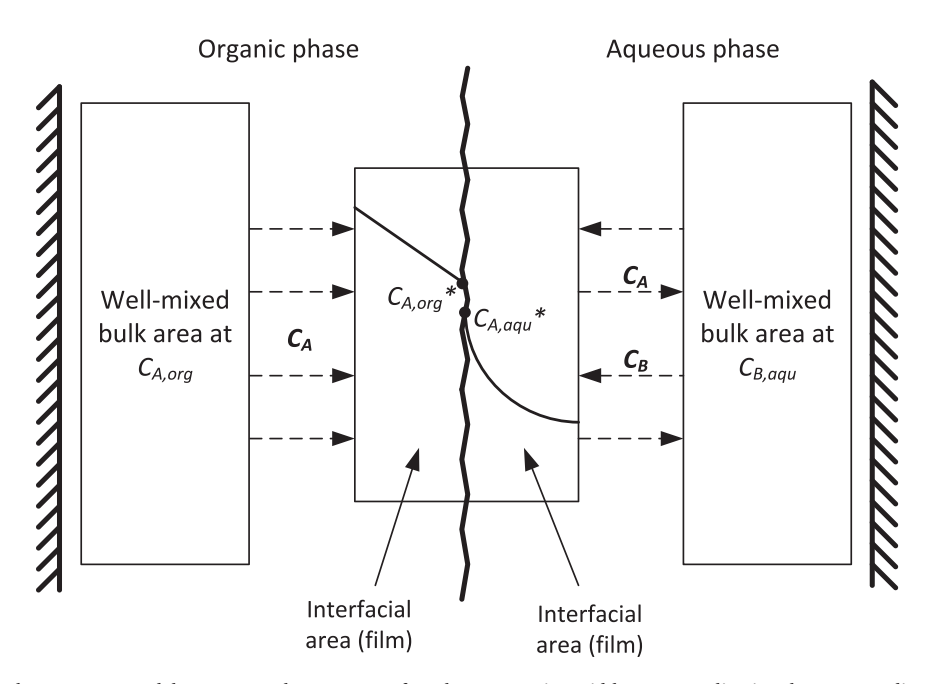


Fig. 11. Surface renewal theory as a model to approach mass transfer phenomena in acid-base neutralization between sodium hydroxide solutions and CCl₃COOH-toluene.

discharge of 40 ml/hour), and a circular silicone channel ($I\!D=1$ mm). These experiments confirm that the slug dimensions, channel material, volumetric flow rate, and the organic-to-aqueous flow rate ratio influence the mass transfer coefficient.

Declaration of Competing Interest

The authors declare that they have no known competing financial interests or personal relationships that could have appeared to influence the work reported in this paper.

Acknowledgment

The author expresses his gratitude for the financial support from the University of Surabaya Research and Community Service Institute (LPPM), Indonesia.

References

- Antony, R., Giri Nandagopal, M.S., Sreekumar, N., Rangabhashiyam, S., Selvaraju, N., 2014. Liquid-liquid slug flow in a microchannel reactor and its mass transfer properties a review. Bull. Chem. React. Eng. Catal. 9 (3), 207–223. https://doi.org/10.9767/bcrec.9.3.6977.207-223.
- Basher, H.O., 2021. Analysis of the heat transfer enhancement in triangular microchannel with a trapezoidal corrugated surface and hybrid nanofluid. Int. J. Heat. Technol. 39 (6), 1721–1732. https://doi.org/10.18280/ijht.390604.
- Christie, J., Geankoplish, 1993. Transport Processes and Unit Operations, 3rd edition. Prentice-Hall, Inc, Englewood Cliffs, N.J., USA. ISBN-81-203-1134-5.
- Dessimoz, A.L., Cavin, L., Renken, A., Kiwi-Minsker, L., 2008. Liquid-liquid two-phase flow patterns and mass transfer characteristics in rectangular glass microreactors. Chem. Eng. Sci. 63 (16), 4035–4044. https://doi.org/10.1016/j.ces.2008.05.005.
- Dessimoz, A.L., Cavin, L., Renken, A., Kiwi-Minsker, L., 2008. Liquid-liquid two-phase flow patterns and mass transfer characteristics in rectangular glass microreactors. Chem. Eng. Sci. 63 (16), 4035–4044. https://doi.org/10.1016/j.ces.2008.05.005.
- Feng, Y., Lee, Y., 2019. Microfluidic fabrication of wrinkled protein microcapsules and their nanomechanical properties affected by protein secondary structure. J. Food Eng. 246 (2018), 102–110. https://doi.org/10.1016/j.jfoodeng.2018.10.028.
- Ghaini, A., Kashid, M.N., Agar, D.W., 2010. Effective interfacial area for mass transfer in the liquid-liquid slug flow capillary microreactors. Chem. Eng. Process.: Process. Intensif. 49 (4), 358–366. https://doi.org/10.1016/j.cep.2010.03.009.
- Jähnisch, K., Hessel, V., Löwe, H., Baerns, M., 2004. Chemistry in microstructured reactors, 43 (4). https://doi.org/10.1002/anie.200300577.
- Jamil, M.F., et al., 2016. Transesterification of mixture of castor oil and sunflower oil in millichannel reactor: FAME yield and flow behaviour. Procedia Eng. 148, 378–384. https://doi.org/10.1016/j.proeng.2016.06.487.
- Jensen, K.F., 2017. Flow chemistry—Microreaction technology comes of age. AIChE J. 63 (3), 858–869. https://doi.org/10.1002/aic.15642.
- Ji, G., Ding, J., Zhong, Q., 2020. Microreactor technology for synthesis of ethyl methyl oxalate from diethyl oxalate with methanol and its kinectics. Can. J. Chem. Eng. 98 (11), 2321–2329. https://doi.org/10.1002/cjce.23775.
- A.V. Kovalev and A.A. Yagodnitsyna, Viscosity Ratio Influence on Liquid-Liquid Flow in a T-shaped Microchannel, no. 2, pp. 365–370, 2021, doi: 10.1002/ceat.202000396.
- Liu, Y., Zhao, Q., Yue, J., Yao, C., Chen, G., 2021. Effect of mixing on mass transfer characterization in continuous slugs and dispersed droplets in biphasic slug flow

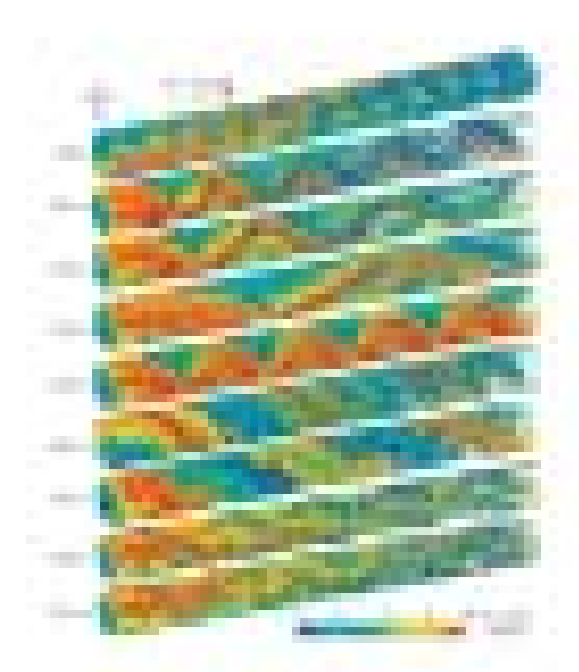
- microreactors. Chem. Eng. J. 406 (2020), 126885 https://doi.org/10.1016/j.cei.2020.126885.
- A. Mazubert, Selection, Development and Design of a Continuous and Intensified Reactor Technology To Transform Waste Cooking Oil in Biodiesel and Biosourced Formulations, pp. 1–192, 2014.
- Melo-Espinosa, E.A., et al., 2014. Surface tension prediction of vegetable oils using artificial neural networks and multiple linear regression. Energy Procedia 57, 886–895. https://doi.org/10.1016/j.egypro.2014.10.298.
- Plutschack, M.B., Pieber, B., Gilmore, K., Seeberger, P.H., 2017. The Hitchhiker's Guide to Flow Chemistry â¥. Sep. 27. In: Chemical Reviews, 117. American Chemical Society, pp. 11796–11893. https://doi.org/10.1021/acs.chemrev.7b00183.
- Prakash, R., Ghosh, S., Feb. 2021. Effect of Bend Wettability on Hydrodynamics of Liquid-Liquid Two-phase Flow in Serpentine Mini Geometry. Ind. Eng. Chem. Res. 60 (7), 3142–3155. https://doi.org/10.1021/acs.iecr.0c05279.
- Ratchananusorn, W., Semyonov, D., Gudarzi, D., Kolehmainen, E., Turunen, I., Nov. 2011. Hydrodynamics and mass transfer studies on a plate microreactor. Chem. Eng. Process.: Process.Intensif. 50 (11–12), 1186–1192. https://doi.org/10.1016/j.cep.2011.08.010.
- Suerz, R., et al., 2021. Application of microreactor technology to dehydration of bioethanol. Chem. Eng. Sci. 229, 116030 https://doi.org/10.1016/j.ces.2020.116030.
- Tiwari, A., Rajesh, V.M., Yadav, S., 2018. Biodiesel production in micro-reactors: a review. Energy Sustain. Dev. 43 https://doi.org/10.1016/j.esd.2018.01.002.
- Tsaoulidis, D., Dore, V., Angeli, P., Plechkova, N.V., Seddon, K.R., 2013. Flow patterns and pressure drop of ionic liquid-water two-phase flows in microchannels. Int. J. Multiph. Flow. vol. 54, 1–10. https://doi.org/10.1016/j. ijmultiphaseflow.2013.02.002.
- N. Volkel, A.Y. Widianto, J. Aubin, and C. Xuereb, Gas-Liquid Taylor Flow Characteristics in Straight and Meandering Rectangular Microchannels, 2008. [Online]. Available: https://aiche.confex.com/aiche/s08/techprogram/P105713.HTM.
- Wang, K., Li, L., Xie, P., Luo, G., 2017. Liquid-Liquid Microflow Reaction Engineering, Reaction Chemistry and Engineering, 2. Royal Society of Chemistry, pp. 611–627. https://doi.org/10.1039/c7re00082k.
- Wang, X., et al., 2020. Scale-up of microreactor: Effects of hydrodynamic diameter on liquid-liquid flow and mass transfer. Chem. Eng. Sci. 226 https://doi.org/10.1016/j. ces 2020.115838
- Wu, L., Huang, K., Wei, T., Lin, Z., Zou, Y., Tong, Z., 2016. Process intensification of NaOH-catalyzed transesterification for biodiesel production by the use of bentonite and co-solvent (diethyl ether). Fuel 186, 597–604. https://doi.org/10.1016/j. fuel.2016.08.106.
- Xu, B., Cai, W., Liu, X., Zhang, X., Jul. 2013. Mass transfer behavior of liquid-liquid slug flow in circular cross-section microchannel. Chem. Eng. Res. Des. 91 (7), 1203–1211. https://doi.org/10.1016/j.cherd.2013.01.014.
- Yao, C., Liu, Y., Xu, C., Zhao, S., Chen, G., Jan. 2018. Formation of liquid–liquid slug flow in a microfluidic T-junction: effects of fluid properties and leakage flow. AIChE J. 64 (1), 346–357. https://doi.org/10.1002/aic.15889.
- Yao, C., Ma, H., Zhao, Q., Liu, Y., Zhao, Y., Chen, G., Sep. 2020. Mass transfer in liquid-liquid Taylor flow in a microchannel: Local concentration distribution, mass transfer regime and the effect of fluid viscosity. Chem. Eng. Sci. 223 https://doi.org/10.1016/j.ces.2020.115734.
- Yeh, C.H., Chen, K.R., Lin, Y.C., 2013. Developing heatable microfluidic chip to generate gelatin emulsions and microcapsules. Microfluid Nanofluidics 15 (6), 775–784. https://doi.org/10.1007/s10404-013-1193-x.
- Zhang, Q., Liu, H., Zhao, S., Yao, C., Chen, G., Feb. 2019. Hydrodynamics and mass transfer characteristics of liquid–liquid slug flow in microchannels: the effects of temperature, fluid properties and channel size. Chem. Eng. J. 358, 794–805. https://doi.org/10.1016/j.cej.2018.10.056.
- Zhang, X., Chen, D., Wang, Y., Cai, W., 2012. Liquid-liquid two-phase flow patterns and mass transfer characteristics in a circular microchannel. Adv. Mater. Res. 89–94. https://doi.org/10.4028/www.scientific.net/AMR.482-484.89.



Chemical Engineering Research and Design

(Black prints with Engage Substitute of District Expressing Sec.).

Service SAS Phys SASA



Expert stage from fractional stady on fractively assess not expected top a positive of stady, because that in a report of the state of the combination and if it is not stated, as using those, beginning there is they long fraction beginning the contract on the general as they are the later.





Chemical Engineering Research and Design

Editor-in-Chief Professor Jerry Heng, Imperial College London, UK

Editorial Board

Professor Bradley Ladewig, University of Luxembourg, Luxembourg Social Media Editor

Professor Eva Sorensen (Topic Coordinator), University College London, UK Distillation and Absorption

Professor Elisabetta Brunazzi, University of Pisa, Italy Dr Tony Cai, Fractionation Research, Inc. (FRI), USA

Professor Jens-Uwe Repke, Technische Universität Berlin, Germany

Dr Joëlle Aubin (Topic Coordinator), University of Toulouse, France Fluid Flow

Dr Giorgio Besagni, Politecnico di Milano, Italy

Professor Farhad Ein-Mozaffari, Ryerson University, Canada Professor Nicky Eshtiaghi, RMIT University, Australia

Dr Xuhong Guo, East China University of Science & Technology, China

Dr Yixiang Liao, Institute of Fluid Dynamics of Helmholtz-Zentrum Dresden – Rossendorf (HZDR), Germany

Professor Mark Simmons, University of Birmingham, UK

Professor Ron Zevenhoven (Topic Coordinator), Åbo Akademi University, Finland Heat and Mass Transfer

Professor Rufat Abiev, St. Petersburg State Institute of Technology Professor Fouad Azizi, American University of Beirut, Lebanon Dr Amol Kulkarni, CSIR-National Chemical Laboratory, Pune, India

Dr Jason Stafford, University of Birmingham, UK

Materials Processing and Product Developmen

Professor Críspulo Gallegos (Topic Coordinator), Universidad de Huelva, Spain

Dr Emmanuel Menya, Gulu University, Uganda

Dr Meenesh Singh, University of Illinois at Chicago, USA

Particle Technology Professor Massimo Poletto (Topic Coordinator), University of Salerno, Italy

Professor Alberto Di Renzo, University of Calabria, Italy Professor Jerry Heng, Imperial College London, UK

Professor Álvaro Ramírez-Gómez, Technical University of Madrid, Spain

Professor Richard Williams, Heriot Watt University, UK

Professor Jerry Heng (Topic Coordinator), Imperial College London, UK Pharmaceutical Engineering

Professor Pui Lai Rachel Ee, National University of Singapore, Singapore

Professor Richard Lakerveld, The Hong Kong University of Science and Technology (HKUST), Hong Kong

Dr Aniruddha Majumder, University of Aberdeen, Aberdeen, UK

Professor Ka Ming Ng, Hong Kong University of Science and Technology, Hong Kong

Dr Nandkishor Nere, AbbVie, Chicago, USA

Process Systems Engineering Professor Michael C. Georgiadis (Topic Coordinator), Aristotle University of Thessaloniki, Greece

Dr Antonio del Rio Chanona, Imperial College London, UK,

Professor Panagiotis Christofides, University of California, Los Angeles, USA Professor Patricia Hoch, Universidad Nacional Del Sur, Argentina Professor Anton A. Kiss, Delft University of Technology, Delft, The Netherlands

Professor Andrzej Kraslawski, Lappeenranta University of Technology, Finland

Dr Pei Liu, Tsinghua University, China

Professor Artur M. Schweidtmann, TU Deflt, The Netherlands

Professor Nilay Shah, Imperial College London, UK Dr Mirko Skiborowski, TU Dortmund, Germany

Professor Thierry Meyer (Topic Coordinator), Swiss Federal Institute of Technology, Switzerland Reaction Engineering

Professor Asterios Gavrillidis, University College London, UK Professor Kai-Olaf Hinrichsen, TU München, Germany Professor Anastasia Macario, University of Calabria, Italy Professor Kyriaki Polychronopoulou, Khalifa University, UAE

Professor Nor Aishah Saidina Amin , Universiti Teknologi Malaysia, Malaysia

Professor Enrico Tronconi, Politecnico di Milano, Italy

Separation Processes Professor Marisa Masumi Beppu (Topic Coordinator), Universidade Estadual de Campinas, São Paulo, Brazil

Professor Xianshe Feng (Topic Coordinator), University of Waterloo, Canada

Professor Yan Wang (Topic Coordinator), Huazhong University of Science and Technology, China.

Dr Moises Bastos-Neto, Universidade Federal de Ceará, Brazil Dr Woei Jye Lau, Universiti Teknologi Malaysia (UTM), Malaysia Dr Asim Khan, COMSATS University Islamabad, Pakistan

Dr Hanna Knuutila, Norwegian University of Science & Technology, NTNU, Norway

Professor Bradley Ladewig, University of Luxembourg, Luxembourg

Dr Ana Mafalda Ribeiro, University of Porto, Portugal

Professor Juan Gabriel Segovia-Hernandez, Universidad de Guanajuato, Mexico

Professor Aiqin Wang, Lanzhou Institute of Chemical Physics, Chinese Academy of Sciences, China

Professor Yan Wang, Huazhong University of Science and Technology, China.

© 2024 The Institution of Chemical Engineers (A Registered Charity in England and Wales and a charity registered in Scotland (SC 039661)). Published by Elsevier B.V. All rights are reserved, including those for text and data mining, Al training, and similar technologies.

[©] The paper used in this publication meets the requirements of ANSI/NISO Z39.48-1992 (Permanence of Paper)

IChemE www.icheme.org/cherd Volume 205, May 2024 ISSN 0263-8762

Chemical Engineering Research and Design

Official journal of the European Federation of Chemical Engineering: Part A

Contents

Distillation and Absorption	174	Initial carbon capture pilot study in Solvay soda ash process A. Krótki, T. Spietz, S. Dobras, T. Chwoła, A. Tatarczuk, D. Żórawski, K. Skowron, Ł. Kiedzik, B. Kowalska and D. Skrzyniecki
	443	Entrainer selection using the Infinitely Sharp Split method and thermodynamic criteria for separating binary minimum-boiling azeotrope by extractive distillation I. Rodriguez-Donis, N. Shcherbakova, E. Parascandolo, J. Abildskov and V. Gerbaud
	598	Hybrid process for separation of morpholine—water mixture: A rigorous design with experimental confirmation based on LLE and VLE data N.V. Rane, H.S. Chitturi, V. Aniya and A. Kumari
Fluid Flow	91	Hydrodynamics and mass transfer performance of microbubble flow in the bubble column with a contraction section X. Liu, M. Lei, Z. Wang, S. Yuan, Q. Li and Z. Wang
	118	The practical meaning of the classical optimizing method and Angular Detection Photometer (ADP) in coagulation tests of surface water B. Libecki, R. Wardzyńska, S. Kalinowski, A. Bęś and A. Szypulska
	188	Modifying the gas-oil ratio and water cut of a PVT lookup table using correlations for fluid volatility CM. Carstensen and S.K. Kanstad
	221	Effect of surfactant adsorption on the efficiency of drainage displacement at different viscosity ratios: A lattice Boltzmann study
	232	T.R. Zakirov, A.S. Khayuzkin and M.G. Khramchenkov Study on the mobility control ability of a quaternary ammonium salt active polymer for oil flooding Q. Chen, M. Ye, X. Nie, W. Pu and J. Hu
	268	Enhanced photoelectrochemical water splitting via 3D flow field structure: Unveiling the decisive role of interfacial mass transfer B. Wang, S. Yang, Y. Lai, Z. Gao and J. Su
	376	Falling, deformation, and coalescence of droplet in model waxy oil under an electric field
		D. Yang, M. Li, Q. Yun, H. Sun, Q. Li, X. Gao, C. Chen and L. He
	401	Process intensification in flow chemistry using micro and millidevices: Numerical simulations of the syntheses of three different intermediate API compounds for diabetes mellitus drug production
		J.L. Silva Jr., P.V.C. Calvo, M.S.A. Palma, M.G.M. Lopes and H.S. Santana
	413	The effect of non-uniform inlet boundary conditions on the performance of the multiphase pump
		C. Peng, Y. Zhang, Y. Pan, X. Shi and Y. Gong

	46/	numerical study for screening potential reservoirs
	F40	J. Sherratt, A. Sharifi Haddad and R. Rafati
	510	Revisiting RANS turbulence modelling for bubble-induced turbulence: Effects of surfactants
		Y. Liao, H. Hessenkemper, D. Lucas and T. Ma
	538	A review of emulsion flows, their characterization and their modeling in pumps
		L. Achour, M. Specklin, M. Asuaje, S. Kouidri and I. Belaidi
	556	Numerical study on hydrodynamics, mixing and heat transfer of highly viscous fluid in a novel shell-and-tube heat exchanger with X-type baffles <i>J. Wang, J. Wang and LF. Feng</i>
	569	Modelling supercritical ${\rm CO_2}$ flow in a co-rotating twin screw extruder using the level-set method
		T.M. Kousemaker, P. Druetta, F. Picchioni and A.I. Vakis
	619	Study on jetting droplet formation regime in a low-speed annular shear flow field
		P. Zou, M. Zhang, Y. Guo, D. Yao and L. Zhang
	733	A simplified drop breakage model for emulsion-producing fluidic devices: Application to fluidic oscillator, helical coil and vortex-based cavitation device
		D.K. Pandey, A.H. Thaker and V.V. Ranade
	748	Pressure drop model of gas-liquid phase for Venturi scrubber in fog- annular flow
		R. Cao, H. Wang, R. Gong, Z. Jiang, H. Zhang, J. Zhu and Y. Song
	802	Study on the safety of a magnetic strainer at the deaerator outlet under two-phase and large-scale flow fields
		H. Zhang, N. Kong, Y. Song, Z. Niu and C. Peng
Heat and Mass Transfer	57	Mass transfer phenomena of partially miscible liquids under liquid-liquid slug flow in a circular microchannel
		A.Y. Widianto, V. Lorenza, C. Clarisa, R. Valentino, C. Elfa and L. Sapei
	608	Heavy fuel oil pyrolysis: A family of practical kinetic reaction models supported by TGA M.J.Z. Ganji and H. Ghassemi
	792	Liquid – Solid mass transfer characteristics of a heterogeneous reactor made of separated horizontal woven screens impinged by a submerged jet S.M. Fouad, Y.M.S. El-Shazly, H.A. Farag and G.H. Sedahmed
Materials Processing and Product Development	67	Pyrolyzed coal base high surface area and mesoporous activated carbon for methyl violet 2B dye removal: Optimization of preparation conditions and adsorption key parameters
		S.A. Musa, A.S. Abdulhameed, S.N.A. Baharin, Z.A. ALOthman, R. Selvasembian and A.H. Jawad
	301	Process for desulfurization and demineralization of low rank coal using oxidation assisted froth floatation technique W. Ahmad, M. Salman, I. Ahmad and M. Yaseen
	335	One step synthesis of FeO _x magnetic nanoparticles in the microreactor with intensively swirling flows
		R.S. Abiev, A.M. Nikolaev, A.S. Kovalenko, G. Yu.E, N.V. Tsvigun, A.E. Baranchikov, G.P. Kopitsa and O.A. Shilova
	591	Engineering ${\rm MgHPO_4\cdot 3H_2O/Mg(OH)_2}$ composite for boosting ${\rm NH_3}$ adsorption properties
		G. Chen, T. Zhou, M. Zhang, Z. Ding and C. Wang

Particle Technology	578	Use of automation, dynamic image analysis, and process analytical technologies to enable data rich particle engineering efforts at the Drug Substance / Drug Product interface: A case study using Lovastatin
		S. Agrawal, S.H. Rawal, V.R. Reddy and J.M. Merritt
	775	Pressure prediction for air cyclone centrifugal classifier based on CNN-LSTM enhanced by attention mechanism
		W. Li, X. Li, J. Yuan, R. Liu, Y. Liu, Q. Ye, H. Jiang and L. Huang
Pharmaceutical Engineering	354	Yield enhancement and phase behaviors of cyclic peptide drug crystallization in the presence of polyethylene glycol additive S. Pu and K. Hadinoto
	517	Model-based investigation of a novel decontamination technology: Ultrasound assisted aerosolized hydrogen peroxide M.R. Gaddem, Y. Hayashi, B.X. Scholz, H. Futamura, K. Kawasaki and
		H. Sugiyama
Process Systems Engineering	1	Model predictive control of nonlinear processes using transfer learning- based recurrent neural networks
		M.S. Alhajeri, Y.M. Ren, F. Ou, F. Abdullah and P.D. Christofides
	28	Prediction and analysis etching model of anti-glare glass roughness based on machine learning method
		T. Yang, L. Zhu, F. Yang, C. Jiang and L. Xie
	148	Investigation on the integration of supercritical CO_2 cycle with natural gas oxy-fuel combustion power plant L. Cai, L. Tan, Y. Liang, Y. Fu and Y. Guan
	292	Design and optimization of boil-off gas recondensation process by
	232	recovering waste cold energy in LNG regasification terminals
		M. Srilekha and A. Dutta
	364	Impact of intermittent electricity supply on a conceptual process design for microbial conversion of ${\rm CO_2}$ into hexanoic acid
		J. Luo, M. Pérez-Fortes, P. Ibarra-Gonzalez, A.J.J. Straathof and A. Ramirez
	640	Acetone-butanol-ethanol fermentation products recovery: Challenges and opportunities
		S. Rafieyan, M.A. Boojari, A. Setayeshnia, M. Fakhroleslam, E. Sánchez-Ramírez, M.S. Bay and J.G. Segovia-Hernández
	722	Coupling semi-transparent PV PANELS with thin-film PBRs for sustainable microalgal biomass production
		J. Louveau, M. Titica, N.R. Moheimani and J. Pruvost
Separation Processes	39	Efficient bipolar membranes with ${\rm Ti_3C_2T_x}$ nanosheets as advanced catalysts in the interfacial layers for water splitting
		X. Zhang, Y. Li, Y. Yuan, C. Wu, X. Wang, Y. Liu and X. Han
	107	Salt-resistant and antibacterial polyvinyl alcohol/chitosan/silver-loaded graphene oxide electrospun nanofiber membrane for high-efficiency solar-driven desalination
		Q. Kang, Y. Zhai, F. Zhao, L. Yang, Y. Yang, HD. Park, Z. Li, H. Chen and G. Sun
	161	Phosphonium-based ionic liquid immobilised in sodium alginate as a novel adsorbent: Kinetics, thermodynamics, and toxicity study on 2,4-dichlorophenol removal
		J.N. Göde, F.J. Malaret, J.P. Hallett, V. Trevisan and E. Skoronski
	388	Evaluating nano-metal oxide mixed matrix membranes for whey protein separation using hybrid intelligent optimization learning
		L.T. Yogarathinam, J. Usman, S.I. Abba, D. Lawal, N. Baig and I.H. Aljundi
	529	Bench and pilot scale assessment of 5A molecular sieves for tail gas treatment applications
		C. Zhu, S. Zhang, W. Zhu, Q. Song, J. Zhang, Y. Weng, Q. Sun, S.A. Duval, R.M. Al Othman, G.P. Lithoxoos and Y. Zhang

	763	Smart ion exchange membrane with high impact in heavy metals separation prepared by electrospinning process with ultrasensitive responsiveness for water treatment S. Bandehali, A. Moghadassi, S.M. Hosseini, F. Parvizian, D. Ghanbari, R. Rahimizadeh and A.A. Ebrahimi
Reaction Engineering	13	Removal routes of hazardous sodium oxalate in the alumina industry based on Bayer process: A review H. Duan, J. Ran, J. Zhao, S. Li, Y. Chen, S. Yin and L. Zhang
	79	Experimental and kinetic modelling studies for the design of fixed bed methanol reactor over CuZA catalyst
	207	F.M. Bagwan, P. Dongapure, A.A. Kulkarni and S.N. Vasireddy
	207	Physicochemical exploration of castor seed oil for high-quality biodiesel production and its sustainable application in agricultural diesel engines S. Phewphong, W. Roschat, T. Ratchatan, W. Suriyafai, N. Khotsuno, C. Janlakorn, T. Leelatam, K. Namwongsa, P. Moonsin, B. Yoosuk, P. Janetaisong and V. Promarak
	246	CPFD simulations of corn stalk gasification in a circulating fluidized bed
		H. Liu, Z. Wang, Y. Huang, M. Zhou, C. Jia, Z. Gu, B. Sun and Q. Wang
	257	Full-period operation optimization of the semi-regenerative reactor based on dehydrogenation reaction and deactivation kinetics H. Jiang, Y. Chu and X. Du
	312	Combination of linear solvation energy and linear free-energy relationships to aid the prediction of reaction kinetics: Application to the solvolysis of 5-HMF by alcohol to levulinate
		E.E. Munoz, D. Di Menno Di Bucchianico, C. Devouge-Boyer, J. Legros, C. Held, JC. Buvat, V.C. Moreno and S. Leveneur
	324	Dissolution behavior and kinetics of copper slag under oxidative conditions
		M.D. Turan, Z.A. San, H. Nizamoğlu and T. Özcan
	459	The effect of Ni- and Mo-based materials on thermochemical sulfate reduction by glycerol under hydrothermal process conditions C. Chang, F. Vogel, O. Kröcher and D. Baudouin
	713	In–situ modification of UiO–66(Zr) organic ligand to synthesize highly recyclable solid acid for biodiesel production H. Li, T. Wang, H. Chu, S.L. Rokhum, Y. Zhang, H. Yu, Q. Xiao, M. Guo, X. Ma, S. Li
Articles from the	47	and G. Li Comparing different single milk droplet drying process with spray drying
Special Issue '10th International Granulation Workshop'		process X. Li, R.B. Al-Asady, C. Sanders and A.D. Salman
•	280	Investigation of the homogeneity of particle suspension Z. Wang, C. Sanders, R.B. Al-Asady and A.D. Salman
Articles from the Special Issue '17th European Conference on Mixing'	486	Fluid dynamics and mixing in a novel intermittently rotating bioreactor for CAR-T cell therapy: Spin-down from incomplete spin-up G.G. Atanasova, A. Ducci and M. Micheletti
J	498	A CFD study on the change of scale of non-Newtonian stirred digesters at low Reynolds numbers
	600	F. Maluta, F. Alberini, A. Paglianti and G. Montante
	628	A dynamic compartment model for spatially heterogeneous reactors: Scalar and Monte-Carlo particle mixing J. Morchain, C. Mayorga, P. Villedieu and A. Liné
		7. Mordiani, G. Mayorga, 1. Vineulea ana A. Line

	665 695	Advanced control of microstructure in ice cream by agitation and mixing during freezing process H. Masuda, T. Ryuzaki, R. Kawachi and H. Iyota Experimental analysis of lifelines in a 15,000 L bioreactor by means of Lagrangian Sensor Particles S. Hofmann, L. Buntkiel, R. Rautenbach, L. Gaugler, Y. Ma, I. Haase, J. Fitschen, T. Wucherpfennig, S.F. Reinecke, M. Hoffmann, R. Takors, U. Hampel and M. Schlüter
	822	Local analysis of micro mixing for the Villermaux-Dushman protocol by using the imaging UV-Vis spectroscopy T. Frey, F. Kexel, M. Grabellus, X.M. Le, M. Hoffmann, F. Herbstritt, M. Grünewald and M. Schlüter
	830	Design and scale up of a mixing process for a novel automotive coating H. Yu, S. Tsochataridou, K. Parsons, R. Kehn, R. Grenville, C.D. Rielly and N.G. Özcan-Taşkın
Articles from the Special Issue 'Chemical Engineering in the Middle East – Challenges and Opportunities'	433	Investigation of controlled autoxidation of HVGO to produce carbon fibres precursors: Role of oxygen availability and mixing L.S. Mohamed, M.M. Hossain and M.N. Siddiquee
	672	Development of multiple explicit data-driven models for accurate prediction of CO ₂ minimum miscibility pressure S. Alatefi, O.E. Agwu, R.A. Azim, A. Alkouh and I. Dzulkarnain
Articles from the Special Issue '9th International Symposium on Hydrogen Energy, Renewable Energy and Materials (HEREM 2023)'	343	Study on characteristics of toluene/chlorobenzene nitrification in different microreactors BC. Han, YD. Chen, HW. Zou, GG. Yu, C. Sheng and GZ. Wang
Articles from the Special Issue "Challenges and Opportunities in Advanced Processes based on Distillation for Sustainable Processes"	131	Novel dynamic control structure of reactive distillation process for isopropanol production via transesterification X. Geng, D. Xu, Z. Hou, H. Li and X. Gao

Journal Rankings

Journal Value Country Rankings

Viz Tools

Help

About Us



Chemical Engineering Research and Design

COUNTR	RY	SUBJECT AREA AND CATEGORY	PUBLISHER	SJR 2024
United I	Kingdom	Chemical Engineering Chemical Engineering (miscellaneous)	Institution of Chemical Engineers	0.728 Q2
	Universities and research institutions in United Kingdom	Chemistry Chemistry (miscellaneous)		H-INDEX
	Media Ranking in United Kingdom			135
PUBLICA	ATION TYPE	ISSN	COVERAGE	INFORMATION
Journal	ls	02638762, 17443563	1983-2025	Homepage
				How to publish in this journal
				cherd@elsevier.com
←	Ads by Google			
	Ad options			
	Send feedback			
	Why this ad? ①			

SCOPE

ChERD aims to be the principal international journal for publication of high quality, original papers in chemical engineering. Papers showing how research results can be used in chemical engineering design, and accounts of experimental or theoretical research work bringing new perspectives to established principles, highlighting unsolved problems or indicating directions for future research, are particularly welcome. Contributions that deal with new developments in plant or processes and that can be given quantitative expression are encouraged. The journal is especially interested in papers that extend the boundaries of traditional chemical engineering.

Q Join the conversation about this journal

FIND SIMILAR JOURNALS ②

1 Chemical Engineering and Technology DEU

79% similarity

2 Chemical Engineering and Processing - Process NLD

77% similarity

3 Reviews in Chemical Engineering DEU

74% similarity

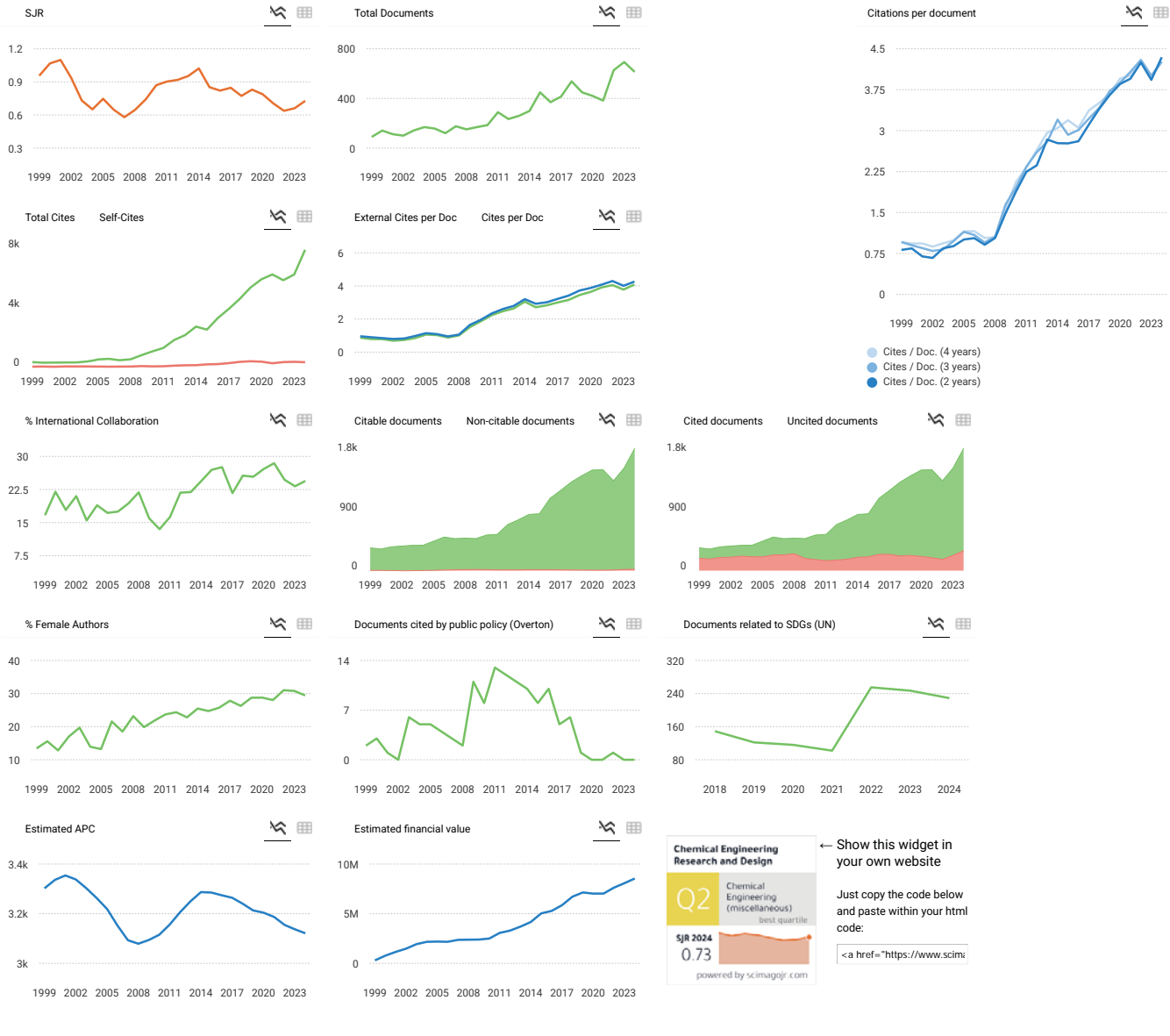
4 International Journal of Chemical Reactor DEU

73% similarity

5 Chinese Journal of Chemical Engineering CHN

options :

71% similarity



G SCImago Graphica

Explore, visually communicate and make sense of data with our new data visualization tool.



Metrics based on Scopus® data as of March 2025

S suresh suresh 6 years ago

i want to updates from this journal

reply



Melanie Ortiz 6 years ago

Dear Suresh,

SCImago Team

Thank you for contacting us. Our data come from Scopus, they annually send us an update of the data. This update is sent to us around April / May every year. Thus, the indicators for 2019 will be available in June 2020 and before that we can't know what will

happen with this journal. Best Regards, SCImago Team

Leave a comment Name Email (will not be published)

Submit

The users of Scimago Journal & Country Rank have the possibility to dialogue through comments linked to a specific journal. The purpose is to have a forum in which general doubts about the processes of publication in the journal, experiences and other issues derived from the publication of papers are resolved. For topics on particular articles, maintain the dialogue through the usual channels with your editor.

Developed by:

SCImago

Powered by:

Follow us on @ScimagoJR

Scimago Lab, Copyright 2007-2025. Data Source: Scopus®

EST MODUS IN REBUS

Legal Notice

Privacy Policy